

Preparation of nickel nanoparticles with different sizes and structures and catalytic activity in the hydrogenation of *p*-nitrophenol

Aili Wang, Hengbo Yin,* Min Ren, Huihong Lu, Jinjuan Xue and Tingshun Jiang

Received (in Victoria, Australia) 10th November 2009, Accepted 4th January 2010

First published as an Advance Article on the web 12th February 2010

DOI: 10.1039/b9nj00657e

Spherical nickel nanoparticles with different sizes and different crystal structures were prepared by reducing nickel oxalate with hydrazine hydrate in the presence of PEG 200, PEG 6000, Tween 40, Tween 80, and sodium dodecyl sulfonate as organic modifiers. The organic modifiers with different functional groups play an important role in deciding the size and structure of the nickel nanoparticles. As compared to the conventional RANEY[®] Ni catalyst, all the as-prepared nickel nanoparticles showed high catalytic activity and selectivity in the hydrogenation of *p*-nitrophenol to *p*-aminophenol. The catalytic activities of the as-prepared nickel nanoparticles generally increased with decreasing the particle size. The crystal structure of nickel nanoparticles also had an important impact on the catalytic activity.

Introduction

Conventionally, *p*-aminophenol, as an important chemical intermediate in the preparation of analgesic and antipyretic drugs,¹ dyestuffs,² and photographic developers,³ is produced by iron-acid reduction of *p*-nitrophenol. In this process, the generation of a large amount of Fe–FeO sludge (1.2 kg kg⁻¹ product) causes a serious pollution problem.⁴ Now the production of *p*-aminophenol is mainly *via* a single step catalytic hydrogenation of nitrobenzene using both noble metal (Pt) and strong mineral acid (H₂SO₄) as co-catalysts.^{4,5} The disadvantages of this process are that strong corrosive sulfuric acid and high cost noble metal are used and that aniline as a competitive byproduct is largely and unavoidably formed. For these reasons, from both economic and environmental points of view, there has recently been increasing interest in the direct hydrogenation of *p*-nitrophenol to *p*-aminophenol catalyzed by nickel,^{6,7} especially by nickel nanoparticles.^{8–10} However, the catalytic performance of nickel nanoparticles in the hydrogenation of *p*-nitrophenol to *p*-aminophenol was seldom investigated until now. In particular, the study of the effect of size and crystal structure of nickel nanoparticles on their catalytic activities is lacking.

It is well known that organic modifiers are used in the size-controlled synthesis of nanosized metals. In the size-controlled synthesis of nickel nanoparticles, several organic modifiers, such as sodium carboxyl methyl cellulose,¹¹ tetrabutylammonium bromide,^{12,13} sulfonated polybutadiene,¹⁴ and cetyltrimethylammonium bromide,¹⁵ have been used to prepare nickel nanoparticles by wet chemical reduction in aqueous solution^{16–19} or in organic media,^{14,20–25} microemulsion,^{26,27} and hydrothermal^{15,28} techniques. Among these techniques, wet chemical reduction is a facile method. But it is difficult to prepare phase pure nickel nanoparticles in aqueous media

because they are easily oxidized in water,^{13,29} which limits their application. In order to avoid the oxidation of nickel nanoparticles, organic solvents, such as tetrahydrofuran,¹⁴ hexadecylamine,²⁰ ethylene glycol,²¹ and ethanol,²² were used in the synthesis of phase pure nickel nanoparticles by a wet chemical method.

In this paper, we report the synthesis of phase pure nickel nanoparticles *via* a simple chemical reduction route in anhydrous ethanol. The effects of organic modifiers with different functional groups, such as poly(ethylene glycol) 200, poly(ethylene glycol) 6000, Tween 40, Tween 80, and sodium dodecyl sulfonate, on the size and crystal structure of the resultant nickel nanoparticles were investigated. The catalytic performance of nickel nanoparticles in the hydrogenation of *p*-nitrophenol to *p*-aminophenol was studied and compared with that of a conventional RANEY[®] Ni catalyst.

Experimental

Materials

Nickel oxalate (NiC₂O₄·2H₂O, 98.5%), hydrazine hydrate (N₂H₄·H₂O, 85%), poly(ethylene glycol) (PEG, MW = 200 or 6000), Tween 40, Tween 80, sodium dodecyl sulfonate, sodium hydroxide (96%), anhydrous ethanol (99.8%), and *p*-nitrophenol were purchased from the Shanghai Chemical Reagent Co. Ltd. All chemicals were used as received without further purification. Anhydrous ethanol was used as a solvent throughout all the experiments.

Preparation of nickel nanoparticles

Nickel nanoparticles were prepared by reducing nickel oxalate with hydrazine hydrate in the presence of organic modifiers with different functional groups, such as PEG 200, PEG 6000, Tween 40, Tween 80, and sodium dodecyl sulfonate. Typically, the organic modifier (0.37 g, 0.01 M) and nickel oxalate (2.49 g, 0.1 M) were dissolved in the anhydrous ethanol solution (70 mL) by ultrasonic dispersion for 30 min. While

Faculty of Chemistry and Chemical Engineering, Jiangsu University, Xuefu Road 301, Zhenjiang, 212013, China. E-mail: yin@ujs.edu.cn; Fax: +86-511-88791800; Tel: +86-511-88787591

the mixture was heated to 60 °C, an ethanol solution of NaOH (1.0 M, 20 mL) was added dropwise into it to adjust the pH of the reaction solution to 12. After that, hydrazine hydrate ethanol solution (7.5 mL in 10 mL anhydrous ethanol) was added dropwise into the mixture and heated up to 80 °C for 8 h under stirring. The resultant nickel nanoparticles were cooled to room temperature and kept in anhydrous ethanol solution. Nickel nanoparticles were centrifuged and washed with anhydrous ethanol when they were used as the catalysts in the hydrogenation of *p*-nitrophenol.

Preparation of RANEY[®] Ni catalyst

RANEY[®] Ni catalyst was prepared by the following procedure: 1.0 g of Ni–Al alloy with a weight ratio of 47:53 and particle sizes in a range of 38–45 μm was added to an aqueous solution of NaOH (6.0 M, 10 mL) under gentle stirring at 50 °C. After that, the reaction solution was heated to 80 °C and stirred for 1 h. The black precipitate was washed with distilled water to neutrality and then washed with anhydrous ethanol to replace water. The as-prepared RANEY[®] Ni catalyst was kept in anhydrous ethanol.

Catalyst characterization

The as-prepared nickel nanoparticles were characterized by X-ray diffraction (XRD) on a Rigaku, D-max 2200 X-ray diffractometer with Cu-K α radiation at $\lambda = 1.5406 \text{ \AA}$. The crystallite sizes of the Ni (111) in the samples were calculated by using Scherrer's equation: $D = K\lambda/(B\cos\theta)$, where K was taken as 0.89, and B was the full width of the diffraction line at half of the maximum intensity. High resolution transmission electron microscopy (HRTEM) images and the corresponding selected area electron diffraction (SAED) patterns were obtained on a microscope (JEM-2100) operated at an acceleration voltage of 200 kV to characterize the morphologies and the crystal structures of the as-prepared nickel nanoparticles. The TEM specimens were prepared by placing a drop of nickel nanoparticle colloids onto a copper grid coated with a layer of amorphous carbon and evaporating the solvent in air at room temperature. The average particle sizes of the nickel nanoparticles were measured from the TEM images by counting at least 150 individual particles. The average particle sizes of the samples were calculated by a weighted average method according to the individual particle sizes of the all counted particles. Fourier transform infrared (FTIR) spectra were collected on a Fourier transform infrared spectrometer (Nicolet Nexus 470) by KBr pellet technique.

Catalytic hydrogenation of *p*-nitrophenol to *p*-aminophenol

The hydrogenation of *p*-nitrophenol was carried out in a 1000 mL capacity stainless steel autoclave fitted with a magnetically driven impeller. The autoclave was charged with 3.0 g of *p*-nitrophenol dissolved in 150 mL anhydrous ethanol and 0.09 g of as-prepared nickel nanoparticles or RANEY[®] Ni catalyst. Firstly, the autoclave was purged with nitrogen for 10 min. Then hydrogen from a cylinder was introduced and raised to 0.8 MPa. Under stirring at 600 rpm, the reaction was carried out at a temperature of 100 °C for different times. The liquid phase sample was analyzed by high-performance liquid

chromatography (HPLC, Varian ProStar 210) equipped with an ultraviolet detector set at a wavelength of 254 nm and a C18 column (5 μm, 4.6 mm × 250 mm). A mixture of methanol and acetic acid (0.2 wt%) aqueous solution (3:2 v/v) was used as a mobile-phase at a flow rate of 1 mL min⁻¹.

Results and discussion

XRD analysis

Fig. 1 shows the XRD patterns of the samples prepared by using organic modifiers with different functional groups. The diffraction peaks appearing at $2\theta = 44.5, 51.9,$ and 76.5° were indexed as the (111), (200), and (220) planes of the face-centered-cubic (fcc) nickel (JCPDS No. 04-0850), respectively. No impurity diffraction peaks, such as nickel oxides or nickel hydroxides, were detected, indicating that phase pure metal nickel was prepared under the present experimental conditions. The crystallite sizes of the Ni (111) in the samples calculated by using Scherrer's equation were 16.9 nm, 13.1 nm, 19.7 nm, 11.8 nm, and 8.5 nm, respectively, when the samples were prepared by using PEG 200, PEG 6000, Tween 40, Tween 80, and sodium dodecyl sulfonate as organic modifiers (Table 1).

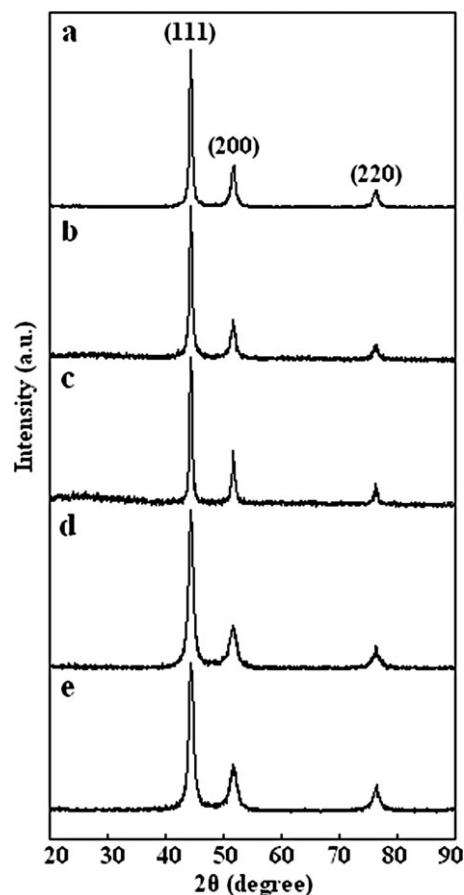


Fig. 1 XRD patterns of nickel nanoparticles prepared by reducing nickel oxalate with hydrazine hydrate and using (a) PEG 200, (b) PEG 6000, (c) Tween 40, (d) Tween 80, and (e) sodium dodecyl sulfonate as organic modifiers, respectively.

Table 1 Crystallite size of Ni (111) (XRD) and average particle size (TEM) of the nickel nanoparticles prepared by using different organic modifiers, and conversion of *p*-nitrophenol at 2 h

Organic modifiers	Crystallite size/nm	Average particle size/nm	Conversion (%)
Tween 40	19.7	297 ± 154.5	14.4
PEG 200	16.9	284 ± 100.5	45.5
PEG 6000	13.1	184 ± 24.6	52.9
Tween 80	11.8	178 ± 19.7	62.6
Sodium dodecyl sulfonate	8.5	60 ± 9.3	80.1

TEM analysis

Fig. 2 shows the TEM and HRTEM images of the nickel nanoparticles prepared by reducing nickel oxalate with hydrazine hydrate in the presence of organic modifiers with different functional groups. Fig. 3 shows the particle size distributions of the as-prepared nickel nanoparticles. The data of the average particle sizes are listed in Table 1.

Fig. 2a shows the TEM image of the nickel nanoparticles prepared by using PEG 200 as an organic modifier. The resultant nickel nanoparticles were sphere-like in shape with an average diameter of *ca.* 284 nm and a size distribution ranging from 67 nm to 733 nm (Fig. 3). The inset shows the SAED pattern obtained by directing the incident electron beam perpendicular to one of the nanoparticles. The diffraction rings are indexed to fcc nickel metal and indicate that the nickel nanoparticles are of a polycrystalline structure. Fig. 2b shows the HRTEM image of the nickel nanoparticles and the inset shows the corresponding inverse fast Fourier transform (FFT) image. It was found that point defects were present in the resultant nickel nanoparticles. Fig. 2c shows the TEM image of nickel nanoparticles prepared by using PEG 6000 as an organic modifier. It was found that the resultant nickel nanoparticles had an average diameter of *ca.* 184 nm and a size distribution ranging from 78 nm to 275 nm (Fig. 3). The inset in Fig. 2c shows the corresponding SAED pattern, indicating that the nickel nanoparticles were of a polycrystalline structure. The HRTEM (Fig. 2d) and FFT images (inset in Fig. 2d, top) show that the resultant polycrystalline nickel nanoparticles had a twin crystal structure. At the same time, the corresponding inverse FFT image (inset in Fig. 2d, bottom) indicates that point defects were also present in the resultant nickel nanoparticles.

Fig. 2e shows the TEM image of the nickel nanoparticles prepared in the presence of Tween 40 as an organic modifier. It was found that the spherical nickel nanoparticles with an average diameter of *ca.* 297 nm and a size distribution ranging from 50 nm to 1000 nm were prepared (Fig. 3). The SAED pattern (inset in Fig. 2e) and the HRTEM image (Fig. 2f) indicate that nickel nanoparticles with a polycrystalline structure were prepared. The inverse FFT image (inset in Fig. 2f, bottom) does not show any defects, indicating that the resultant nickel nanoparticles had a comparatively perfect internal structure. Fig. 2g shows the TEM image of the nickel nanoparticles prepared in the presence of Tween 80 as an organic modifier. The resultant spherical nickel nanoparticles had an average diameter of *ca.* 178 nm and a size distribution ranging from 95 nm to 238 nm (Fig. 3). The corresponding SAED pattern

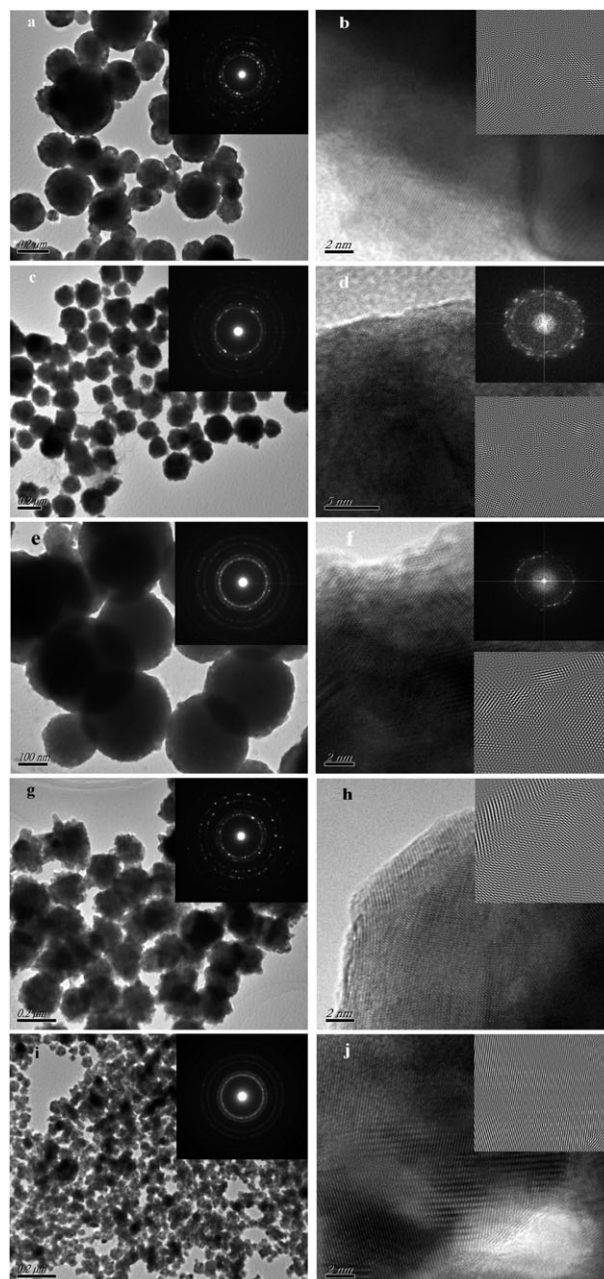


Fig. 2 TEM and HRTEM images of the nickel nanoparticles prepared by reducing nickel oxalate with hydrazine hydrate and using (a, b) PEG 200, (c, d) PEG 6000, (e, f) Tween 40, (g, h) Tween 80, and (i, j) sodium dodecyl sulfonate as organic modifiers, respectively. The insets in the TEM images show the corresponding SAED patterns and the diffraction rings are assigned to {111}, {200}, {220}, and {311} reflections of fcc nickel metal, respectively. The insets in the HRTEM images show the corresponding FFT and inverse FFT images.

(inset in Fig. 2g) indicates that fcc nickel nanoparticles with a polycrystalline structure were formed. The HRTEM and the inset inverse FFT images (Fig. 2h) show that dislocations were present in the resultant nickel nanoparticles.

Fig. 2i shows the TEM image of the nickel nanoparticles prepared in the presence of sodium dodecyl sulfonate as an organic modifier. The resultant spherical nickel nanoparticles had an average diameter of *ca.* 60 nm and a size distribution

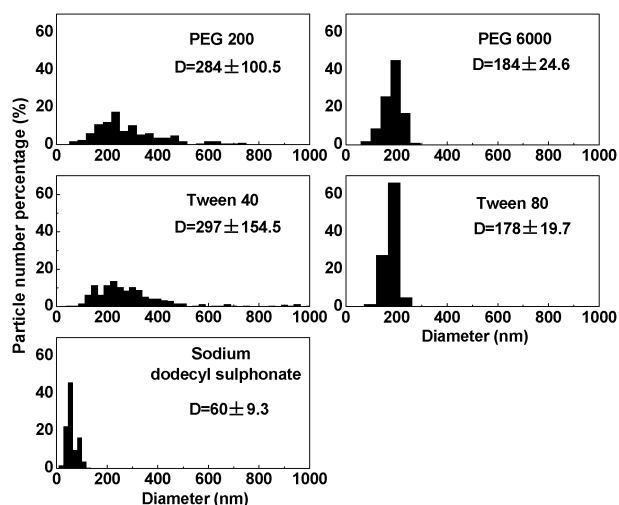


Fig. 3 Particle size distributions of the Ni samples prepared by using PEG 200, PEG 6000, Tween 40, Tween 80, and sodium dodecyl sulfonate as organic modifiers, respectively. D, average particle size.

ranging from 18 nm to 127 nm (Fig. 3). The SAED pattern (inset in Fig. 2i) indicates that fcc nickel nanoparticles with polycrystalline structure were formed. The HRTEM and the inverse FFT image (Fig. 2j) show that dislocations were present in the resultant nickel nanoparticles.

It was found that the average particle sizes of the as-prepared nickel nanoparticles calculated from TEM images are larger than those calculated by using Scherrer's equation. It is reasonable to conclude that all the as-prepared nickel nanoparticles are of polycrystalline structures, consistent with that obtained by SAED analysis.

FTIR analysis

In order to investigate the interaction between the organic modifiers and the nickel nanoparticles, FTIR spectra of the samples were measured. The representative FTIR spectra of the pure organic modifiers and the resultant nickel nanoparticles are shown in Fig. 4.

Fig. 4a and b show the FTIR spectra of pure PEG 6000 and unwashed nickel nanoparticles prepared in the presence of PEG 6000 as an organic modifier. The FTIR spectra of pure PEG 6000 show that the C–O–C stretching vibrations appear at $\nu_{\max}/\text{cm}^{-1}$ 1106 ($\nu(\text{C–O–C})_{\text{trans}}$) and 1148 ($\nu(\text{C–O–C})_{\text{gauche}}$) (Fig. 4a).^{30,31} The appearance of the band at $\nu_{\max}/\text{cm}^{-1}$ 1062 ($\nu(\text{C–O–C})$) in the FTIR spectra of the unwashed sample (Fig. 4b) indicated that the ether bond of PEG 6000 molecules interacted with the surface of the nickel nanoparticles.

Fig. 4c and d show the FTIR spectra of pure Tween 80 and unwashed nickel nanoparticles. In the FTIR spectra of pure Tween 80 (Fig. 4c), the bands appearing at $\nu_{\max}/\text{cm}^{-1}$ 1736 and 1109 are assigned to the stretching vibrations of C=O and C–O–C, respectively.^{32,33} These bands were shifted to $\nu_{\max}/\text{cm}^{-1}$ 1571 (C=O) and 1058 (C–O–C) in the FTIR spectra of the unwashed sample (Fig. 4d), indicating that Tween 80 was adsorbed on the surface of the nickel nanoparticles.

Fig. 4e and f show the FTIR spectra of pure sodium dodecyl sulfonate and unwashed nickel nanoparticles. The bands appearing at $\nu_{\max}/\text{cm}^{-1}$ 1065 and 1056 ($\nu(\text{–SO}_3^-)$) were

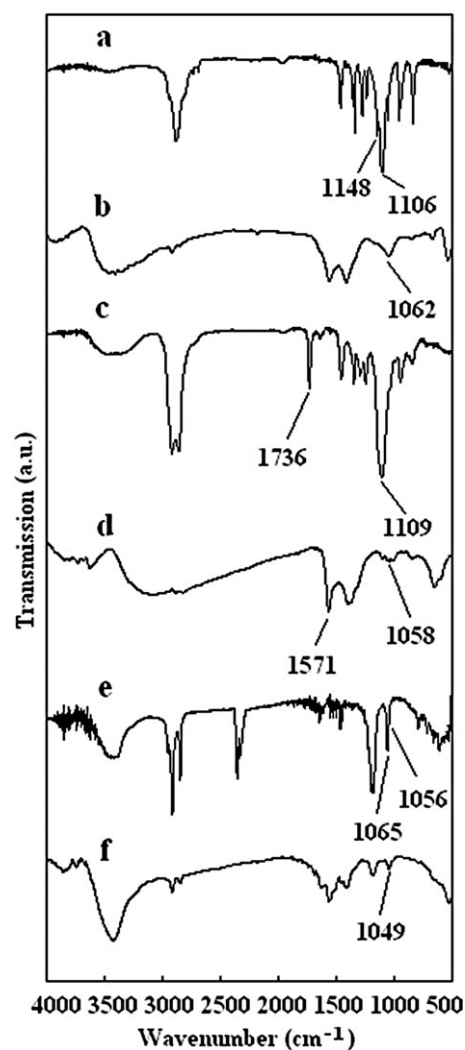


Fig. 4 FTIR spectra of pure (a) PEG 6000, (c) Tween 80, (e) sodium dodecyl sulfonate, and unwashed nickel nanoparticles prepared by reducing nickel oxalate with hydrazine hydrate and using (b) PEG 6000, (d) Tween 80, and (f) sodium dodecyl sulfonate as organic modifiers, respectively.

observed in the FTIR spectra of pure sodium dodecyl sulfonate (Fig. 4e).³⁴ The appearance of the band at $\nu_{\max}/\text{cm}^{-1}$ 1049 ($\nu(\text{–SO}_3^-)$) in the unwashed sample (Fig. 4f) revealed that there was an interaction between the sulfonic group of sodium dodecyl sulfonate and the nickel nanoparticles.

When the as-prepared nickel nanoparticles were washed with anhydrous ethanol, no IR bands of the organic modifiers were observed in the FTIR spectra, meaning that the organic modifiers were completely removed by washing with ethanol. The interaction between organic modifier and nickel nanoparticle affected the particle size and structure.

Catalytic activity

The catalytic activities of the resultant nickel nanoparticles are illustrated in Fig. 5. The selectivity of *p*-aminophenol was 100% while the hydrogenation of *p*-nitrophenol was catalyzed by all the resultant nickel nanoparticles. After the first 2 h, the initial *p*-nitrophenol hydrogenation rates of the nickel

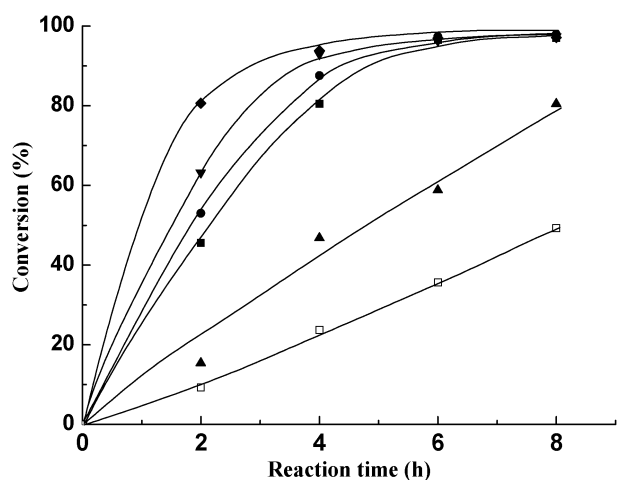


Fig. 5 Catalytic activities of the nickel nanoparticles prepared by reducing nickel oxalate with hydrazine hydrate in the presence of (■) PEG 200, (●) PEG 6000, (▲) Tween 40, (▼) Tween 80, and (◆) sodium dodecyl sulfonate as organic modifiers, respectively, and the (□) RANEY[®] Ni catalyst in the hydrogenation of *p*-nitrophenol to *p*-aminophenol.

nanoparticles were 5.63, 4.40, 3.72, 3.20, and 1.01 mol_{nitrophenol}/mol_{cat}·h, and the *p*-nitrophenol conversions were 80.1%, 62.6%, 52.9%, 45.5%, and 14.4% (Table 1) while the nickel nanoparticles were prepared by using sodium dodecyl sulfonate, Tween 80, PEG 6000, PEG 200, and Tween 40 as organic modifiers, respectively. After reaction for 8 h, the conversions of *p*-nitrophenol were up to 97%, 97%, 98%, 97%, and 80%, respectively. By comparing the initial *p*-nitrophenol hydrogenation rates at the first 2 h, it was found that the catalytic activities of the nickel nanoparticles were in an order of sodium dodecyl sulfonate (60 nm) > Tween 80 (178 nm) > PEG 6000 (184 nm) > PEG 200 (284 nm) ≫ Tween 40 (297 nm). The catalytic activity of the nickel nanoparticles generally increased with decreasing their sizes.

Interestingly, although the nickel nanoparticles prepared by using PEG 200 and Tween 40 as organic modifiers had comparable average particle sizes, the catalytic activity of the former was *ca.* 3.2 times higher than that of the later. As certified by HRTEM analysis, the nickel nanoparticles prepared by using PEG 200 as an organic modifier had point defects. However, when Tween 40 was used as an organic modifier, the as-prepared nickel nanoparticles had a comparatively perfect internal structure. It can be concluded that the catalytic activity of the nickel nanoparticles depends on the synergistic effect of the crystal structure and the size.

To compare the catalytic activities of the as-prepared nickel nanoparticles with that of RANEY[®] Ni catalyst, the catalytic activity of RANEY[®] Ni catalyst was also investigated. The initial *p*-nitrophenol hydrogenation rate of RANEY[®] Ni catalyst was 0.64 mol_{nitrophenol}/mol_{cat}·h after the first 2 h. After reaction for 8 h, the conversion of *p*-nitrophenol was only 49% (Fig. 5). The initial *p*-nitrophenol hydrogenation rate of the nickel nanoparticles was 1.6–8.8 times higher than that of RANEY[®] Ni catalyst. On the other hand, there was a byproduct produced and the selectivity of *p*-aminophenol was less than 95% while *p*-nitrophenol hydrogenation was

catalyzed by RANEY[®] Ni catalyst. The byproduct was ascribed to the product of benzene ring hydrogenation, which was caused by the micropores of RANEY[®] Ni.^{8,35} The results showed that the nickel nanoparticles had higher catalytic activity and selectivity than RANEY[®] Ni catalyst in the hydrogenation of *p*-nitrophenol to *p*-aminophenol.

Conclusions

In summary, nickel nanoparticles with different sizes and different structures were prepared by reducing nickel oxalate with hydrazine hydrate in the presence of organic modifiers, such as PEG 200, PEG 6000, Tween 40, Tween 80, and sodium dodecyl sulfonate, respectively. The ability of the organic modifiers on decreasing particle size of nickel nanoparticles is in an order of sodium dodecyl sulfonate (60 nm) > Tween 80 (178 nm) > PEG 6000 (184 nm) > PEG 200 (284 nm) > Tween 40 (297 nm). PEG 6000 caused the formation of nickel nanoparticles with a twin crystal structure and point defects while PEG 200 resulted in the formation of nickel nanoparticles with point defects. When Tween 80 was used as an organic modifier, the nickel nanoparticles with dislocations were formed. The nickel nanoparticles with a relatively perfect internal structure were prepared in the presence of Tween 40 as an organic modifier. When sodium dodecyl sulfonate was used as an organic modifier, nickel nanoparticles with dislocations were formed. The catalytic activity of the nickel nanoparticles in the hydrogenation of *p*-nitrophenol to *p*-aminophenol generally increased with decreasing their sizes. However, the catalytic activity of nickel nanoparticles depended not only on the size but also on the crystal structure. All the resultant nickel nanoparticles showed higher catalytic activity and selectivity than the RANEY[®] Ni catalyst.

Acknowledgements

The authors would like to thank Professor K. Chen (Jiangsu University) for supporting TEM and HRTEM measurements of nickel samples. This work was financially supported by research funds from Jiangsu Province Education Bureau (1221310008) and Zhenjiang Science and Technology Bureau (GJ2006006) and Jiangsu University (1281310001).

References

- 1 M. Pinza, M. Brufani and C. Milanese, *US Pat.*, 6 043 285, 2000.
- 2 L. Chassot and H. J. Braun, *US Pat.*, 6 592 631 B2, 2003.
- 3 F. Faranda, *US Pat.*, 5 998 110, 1999.
- 4 C. V. Rode, M. J. Vaidya and R. V. Chaudhari, *Org. Process Res. Dev.*, 1999, **3**, 465–470.
- 5 C. V. Rode, M. J. Vaidya, R. Jaganathan and R. V. Chaudhari, *Chem. Eng. Sci.*, 2001, **56**, 1299–1304.
- 6 M. J. Vaidya, S. M. Kulkarni and R. V. Chaudhari, *Org. Process Res. Dev.*, 2003, **7**, 202–208.
- 7 H. Lu, H. Yin, Y. Liu, T. Jiang and L. Yu, *Catal. Commun.*, 2008, **10**, 313–316.
- 8 Y. Du, H. Chen, R. Chen and N. Xu, *Appl. Catal., A*, 2004, **277**, 259–264.
- 9 R. Chen, Q. Wang, Y. Du, W. Xing and N. Xu, *Chem. Eng. J.*, 2009, **145**, 371–376.
- 10 R. Chen, Y. Du, Q. Wang, W. Xing, W. Jin and N. Xu, *Ind. Eng. Chem. Res.*, 2009, **48**, 6600–6607.

- 11 K. H. Kim, Y. B. Lee, S. G. Lee, H. C. Park and S. S. Park, *Mater. Sci. Eng., A*, 2004, **381**, 337–342.
- 12 M. L. Singla, A. Negi, V. Mahajan, K. C. Singh and D. V. S. Jain, *Appl. Catal., A*, 2007, **323**, 51–57.
- 13 D. H. Chen and C. H. Hsieh, *J. Mater. Chem.*, 2002, **12**, 2412–2415.
- 14 A. Nandi, M. D. Gupta and A. K. Banthia, *Mater. Lett.*, 2002, **52**, 203–205.
- 15 E. A. Abdel-Aal, S. M. Malekzadeh, M. M. Rashad, A. A. El-Midany and H. El-Shall, *Powder Technol.*, 2007, **171**, 63–68.
- 16 D. P. Wang, D. B. Sun, H. Y. Yu and H. M. Meng, *J. Cryst. Growth*, 2008, **310**, 1195–1201.
- 17 X. Ni, J. Zhang, Y. Zhang and H. J. Zheng, *J. Colloid Interface Sci.*, 2007, **307**, 554–558.
- 18 K. H. Kim, H. C. Park, S. D. Lee, W. J. Hwa, S. S. Hong, G. D. Lee and S. S. Park, *Mater. Chem. Phys.*, 2005, **92**, 234–239.
- 19 S.-H. Wu and D.-H. Chen, *Chem. Lett.*, 2004, **33**, 406–407.
- 20 Y. Hou and S. Gao, *J. Mater. Chem.*, 2003, **13**, 1510–1512.
- 21 K. Yu, D. J. Kim, H. S. Chung and H. Liang, *Mater. Lett.*, 2003, **57**, 3992–3997.
- 22 L. Bai, F. Yuan and Q. Tang, *Mater. Lett.*, 2008, **62**, 2267–2270.
- 23 F. Alonso, J. J. Calvino, I. Osante and M. Yus, *Chem. Lett.*, 2005, **34**, 1262–1263.
- 24 F. Alonso, J. J. Calvino, I. Osante and M. Yus, *J. Exp. Nanosci.*, 2006, **1**, 419–433.
- 25 G. G. Couto, J. J. Klein, W. H. Schreiner, D. H. Mosca, A. J. A. de Oliveira and A. J. G. Zarbin, *J. Colloid Interface Sci.*, 2007, **311**, 461–468.
- 26 D. E. Zhang, X. M. Ni, H. G. Zheng, Y. Li, X. J. Zhang and Z. P. Yang, *Mater. Lett.*, 2005, **59**, 2011–2014.
- 27 D. H. Chen and S. H. Wu, *Chem. Mater.*, 2000, **12**, 1354–1360.
- 28 C. Wang, X. M. Zhang, X. F. Qian, Y. Xie, W. Z. Wang and Y. T. Qian, *Mater. Res. Bull.*, 1998, **33**, 1747–1751.
- 29 Y. Li, M. Cai, J. Rogers, Y. Xu and W. Shen, *Mater. Lett.*, 2006, **60**, 750–753.
- 30 M. Rozenberg, A. Loewenschuss and Y. Marcus, *Spectrochim. Acta, Part A*, 1998, **54**, 1819–1826.
- 31 Y. Zhou, R. Zhuo and Z. Liu, *Polymer*, 2004, **45**, 5459–54633.
- 32 R. Barreiro-Iglesias, C. Alvarez-Lorenzo and A. Concheiro, *J. Controlled Release*, 2001, **77**, 59–75.
- 33 A. Hillgren, J. Lindgren and M. Aldén, *Int. J. Pharm.*, 2002, **237**, 57–69.
- 34 W. Liu, J. Kumar and S. Tripathy, *Langmuir*, 2002, **18**, 9696–9704.
- 35 D. H. Zuo, Z. K. Zhang and Z. L. Cui, *Chin. J. Mol. Catal.*, 1995, **9**, 298–301.